Boundary-Layer Meteorol (2007) 122:701–719
DOI 10.1007/s10546-006-9121-1

ORIGINAL PAPER

Wind profiles, momentum fluxes and roughness lengths at Cabauw revisited

J. W. Verkaik · A. A. M. Holtslag

Received: 13 March 2006 / Accepted: 3 August 2006 /
Published online: 21 October 2006

Abstract We describe the results of an experiment focusing on wind speed and momentum fluxes in the atmospheric boundary layer up to 200 m. The measurements were conducted in 1996 at the Cabauw site in the Netherlands. Momentum fluxes are measured using the K-Gill Propeller Vane. Estimates of the roughness length are derived using various techniques from the wind speed and flux measurements, and the observed differences are explained by considering the source area of the meteorological parameters. A clear rough-to-smooth transition is found in the wind speed profiles at Cabauw. The internal boundary layer reaches the lowest k-vane (20 m) only in the south-west direction where the obstacle-free fetch is about 2 km. The internal boundary layer is also reflected in the roughness lengths derived from the wind speed profiles. The lower part of the profile (<40 m) is not in equilibrium and no reliable roughness analysis can be given. The upper part of the profile can be linked to a large-scale roughness length. Roughness lengths derived from the horizontal wind speed variance and gustiness have large footprints and therefore represent a large-scale average roughness. The drag coefficient is more locally determined but still represents a large-scale roughness length when it is measured above the local internal boundary layer. The roughness length at inhomogeneous sites can therefore be determined best from drag coefficient measurements just above the local internal boundary layers directly, or indirectly from horizontal wind speed variance or gustiness. In addition, the momentum and heat fluxes along the tower are analysed and these show significant variation with height related to stability and possibly surface heterogeneity. It appears that the dimensionless wind speed gradients scale well with local fluxes for the variety of conditions considered, including the unstable cases.

J. W. Verkaik (✉)
Climate Services and Analysis, Royal Netherlands Meteorological Institute (KNMI),
Wilhelminalaan 10, PO Box 201, 3730 AE De Bilt, the Netherlands
e-mail: job.verkaik@knmi.nl

A. A. M. Holtslag
Meteorology and Air Quality Section, Wageningen University, Wageningen, the Netherlands
e-mail: bert.holtslag@wur.nl

Keywords Cabauw · Drag coefficient · Flux–profile relationship · Footprint area · Gustiness · K-Gill · Local scaling · Roughness length · Wind speed

1 Introduction

We describe an experiment set up to further investigate profiles of wind speed and vertical fluxes, flux–profile relationships, and roughness lengths at relatively high levels in the atmospheric boundary layer (ABL) at Cabauw (The Netherlands). The 213-m high tower offers excellent opportunities for boundary-layer research and many studies have been done on the roughness and flux–profile relationships (Van Ulden and Wieringa 1996, Beljaars and Bosveld 1997). Nieuwstadt (1978) fitted profiles of wind speed and temperature measured along the tower to the flux–profile relationships. In the west direction, the most open sector at Cabauw, he found large discrepancies between the fluxes from the profiles and direct flux measurements. Beljaars (1982) showed that about half of the momentum flux can be attributed to form drag on the wind breaks in the Cabauw environment. Close to the tower the surface is free of obstacles. Consequently, momentum fluxes close to the surface are lower than those aloft and the local roughness length is much smaller than the large-scale roughness length.

Using a small dataset Beljaars et al. (1983) showed that the momentum flux increases 40% between heights of 3.5 m and 22.5 m for wind directions having wind breaks in the upstream terrain. The dimensionless wind speed gradient in the lowest 10 m is closer to literature values when increased by 40% for these directions. Nieuwstadt (1984) used Cabauw data and showed that in the stable boundary layer the dimensionless gradient scales with the local fluxes of momentum and heat instead of the surface fluxes. Holtslag (1984) estimated the momentum and heat fluxes at the surface from data that are available at standard synoptic stations, and estimated wind speed profiles up to 200 m and compared them to observations at the tower. Beljaars (1987b) estimated the large-scale roughness lengths from observations of the standard deviation of the horizontal wind speed in the surface layer and found values between 0.04 m and 0.15 m depending on wind direction.

In the present study we elaborate on the results of Beljaars et al. (1983) using a much larger dataset. We investigate whether the flux–profile relationships are valid in the disturbed boundary layer and explore the use of local scaling in stable and unstable conditions. Note that only a few studies deal with the validation of local scaling of wind and temperature gradients in unstable conditions. Sorbjan (1986) tested local scaling for the dimensionless wind speed (ϕ_m) and temperature gradient (ϕ_h) using a small dataset from Minnesota. Yumao et al. (1997) tested local scaling for ϕ_m and ϕ_h for an urban and a rural site near Nanjing. Recently, Steeneveld et al. (2005) tested local scaling at Cabauw for temperature and humidity profiles.

Although the landscape at Cabauw is fairly open, there are frequent wind breaks and scattered villages, varying in distance and density, causing a strong disturbance of the surface layer (Beljaars 1982). In this paper we test local scaling for ϕ_m at Cabauw and we compare the surface roughness length derived using several methods as a function of wind direction. We investigate how the roughness lengths relate to the vertical fluxes, wind speed profiles and their footprint areas. We re-evaluate the results of Nieuwstadt (1978) and explain the discrepancies he observed between momentum fluxes from profiles and direct flux measurements. Although our flux measurements include sensible heat fluxes as well, we only focus on the wind speed profile and momentum flux. We present results from the summer period of 1996 (May–October) during which the weather conditions were close to their climatological averages.

2 Experiment

The Royal Netherlands Meteorological Institute (KNMI) has conducted ABL observations at the Cabauw site since the early 1970s. The tower is a solid cylinder with 2 m diameter, is 213 m high and has booms in three directions (010°, 130°, 250°) at intervals of 20 m. The booms extend 9.4 m beyond the surface of the cylinder. At the end of the north and south-west pointing booms two lateral extensions (1.5 m) carry four plugs. The routine observations include profiles of meteorological parameters (e.g. wind speed and direction, temperature, moisture) and a number of surface parameters (e.g. radiation, precipitation). Table 1 gives details on the installed instruments (Monna and Van der Vliet 1987, Van der Vliet 1998).

From the routine surface-layer observations the friction velocity (u_* [m s^{-1}]) and sensible heat flux (H [W m^{-2}]) are computed using the flux–profile relationships for homogeneous terrain (Dyer 1974). These observations are referred to as the surface-layer observations (subscript SL). H_{SL} and $u_{*\mathrm{SL}}$ are computed from the wind speed at 10 m, a tabulated effective roughness length relevant for the particular wind direction, and the difference in temperature between 1.5 m and 10 m (Wessels 1984).

The roughness length ($z_{0\mathrm{std}}$ [m]) has been derived from the ratio of the standard deviation of the longitudinal wind speed variations (σ_u) to the wind speed at 10 m height in 10-min averaging periods measured during neutral conditions (Beljaars 1987a, 1988). From $u_{*\mathrm{SL}}$ and H_{SL} the surface-layer stability parameter (Obukhov length) is calculated from $L_{\mathrm{SL}} = -u_{*\mathrm{SL}}^3 \theta c_p \rho / \kappa g H_{\mathrm{SL}}$. Here θ is the temperature [K], ρc_p is the product of the specific heat and density of air [J K^{-1} m^{-3}], and g is the acceleration of gravity [m s^{-2}].

In 1996 the routine measurements were completed with direct momentum and sensible heat flux measurements using K-Gill Propeller Vanes at the tower (subscript KV). The k-vane is an instrument comprising two propellers, one oriented 45° upward, the other 45° downward, and a vane to aim the propellers into the main wind direction; it has been equipped with a thermocouple to measure the heat flux. The k-vane is a first-order response instrument with a response length of 2.9 m; details on the k-vane can be found in Verkaik (1998). The averaging period is 30 min for both the k-vane measurements and the routine Cabauw measurements. Unfortunately, data on the atmospheric boundary layer height are not available for the major part of our dataset.

Table 1 Instrumentation at the Cabauw tower during the summer of 1996

Element	Height (m)	Direction	Instrument
Temperature	0.6, 1.5, 10, 20, 40, 80, 140, 200	south-east	Thermocouple (melting ice reference at 0.6 m and 200 m)
Wind	10, 20, 40, 80, 140, 200	south-west, north	Propeller vane (Gill 8002DX)
Momentum and heat fluxes	20, 100, 180	south-west, north	K-Gill propeller vane (Young 35301)

Wind speed measurements at the tower suffer from flow distortion. For that reason two anemometers are placed at each level, one on the north boom (on the right most plug of the right lateral extension) and one on the south-west boom (on the left most plug on the left lateral extension). The anemometer that is best exposed is used in the analysis. At 20 m and below the building at the base of the tower causes flow distortion as well (Wessels 1983); the octagonal shaped building is 3.8 m high and has a diameter of 17.3 m. For that reason the wind speed measurements at 10 m and 20 m are not made at the main tower but on auxiliary masts 29 m in the south-east and 73 m in the north-west direction of the main tower. However, the flux measurements at 20 m are made at the main tower. Comparison of the momentum and heat flux measurements at each level as a function of wind direction shows that the flow distortion by the tower and the building does not affect the flux measurement significantly, not even at the 20-m level.

When planning the measurement campaign the k-vanes were preferred to sonic 3-D anemometers as they were considered better all-weather flux probes and, at that time, a cheaper alternative. The measurements continued throughout the summer of 1996. Due to frequent malfunctioning of the k-vane's electronics, however, the dataset has many gaps.

3 Terrain description

The Cabauw tower is situated in the central river delta in the south-western part of the Netherlands (52°58′18″ N, 4°55′37″ E). The North Sea is at a distance of 50 km in the north-west direction. Close to the tower the surface consists mainly of short grass (>80%) with several small villages, scattered farms, rows of trees and bushes. Maps of the Cabauw environment have been published in Holtslag (1984), Monna and Van der Vliet (1987), and Van Ulden and Wieringa (1996).

A roughness map of the Cabauw environs is plotted in Fig. 1, and is derived from the land-use map LGN3+ of the Dutch environmental research institute Alterra (De Wit et al. 1999). LGN3+ is a raster file covering the whole of the Netherlands with a resolution of $(25\,\mathrm{m})^2$, and is derived from Landsat-TM satellite images from 1995 and 1997 and from topographical information. Over 40 land-use types are distinguished of which 15 are present in the Cabauw environment. Despite the high resolution of the LGN3+ images, narrow roughness elements such as tree lines may not be distinguished. For example, most roads in the Cabauw environment are lined with trees that are rarely detected. Even so, complex terrain features, like the river banks, are not recognized. To each land-use type a roughness length adopted from the literature is assigned (Wieringa 1993). Note that these roughness lengths usually refer to homogeneous areas, while they are applied to inhomogeneous terrain here.

Figure 1 shows that the only sector that is open and nearly free of obstacles for several kilometres is south-west of the tower. To the north there is a road with houses and trees comprising a windbreak-like obstacle at a minimum distance to the tower of about 0.5 km. Farther upstream pasture continues until again there is a road with houses and trees at about 3 km. To the east is the village Lopik at a distance of 1 km. In this direction the local road continues and so do the built-up areas and trees. To the south-east lies a complex terrain with roads, orchards, and the river bed. From inspection of the land-use map four wind direction sectors are distinguished for the Cabauw site (see Table 2). The dataset will be separated into these wind direction

Fig. 1 Roughness lengths on a grey scale for the Cabauw environment [(10 km)^2]. The circle in the centre of the figure indicates the tower position. Dark areas are smooth, bright areas are rough. Lowest and highest roughness lengths found in this region are approximately 0.001 and 1 m respectively. Pixel size (25 m)^2

Table 2 Wind direction sectors for data analysis

north	315°–045°	regularly spaced wind breaks, 1–2 km spacing, on pasture making a *shelterbelt landscape*
east	45°–105°	a chain of small villages making up a *uniform rough* landscape
south	105°–165°	orchards, dikes and the river bed making up a rather complex, *scattered rough* terrain
west	180°–240°	*nearly smooth, open* landscape

sectors to assess the influence of differences in the upstream terrain on the profiles and fluxes.

4 Dataset

As the k-vanes need air flow to operate properly, only those cases are selected where the wind speed measured at 20 m on the tower and the k-vanes at all levels is equal to or larger than 3 m s^{-1}. Runs with significant precipitation are also excluded, i.e. the amount of precipitation is less than 0.1 mm, and the duration is less than 1 min per 30-min interval. Next, the routine measurements of the wind direction and temperature at 20 m and the friction velocity must be available.

Table 3 shows how the number of 30-min runs available for analysis is reduced by the selection rules. While the highest possible number of 30-min runs in the summer period is 8832, about 2500 momentum flux runs (30% data coverage) and 2000 heat flux runs (25%) are available for analysis at each level. For the determination of the roughness lengths the following additional criteria are used in an attempt to exclude measurements made above the surface layer (Korrell et al. 1982): wind direction turning with height is less than 20°, the friction velocity is larger than 0.15 m s^{-1}, and

Table 3 Data selection rules, number of 30-min runs, and percentages of data coverage

Total	8832	100%
$U_{SL,20} \geq 3\,\mathrm{m\,s^{-1}}$	6163	70%
$\theta_{SL,20}$ and $dd_{SL,20}$ present	5503	62%
no precipitation	5092	58%
u_{*SL} present	4835	55%
$dd_{SL,20}$ within selected directions	3670	42%
$U_{kv} \geq 3\,\mathrm{m\,s^{-1}}$ at each height	≈2500	≈30%

U: wind speed, θ: temperature, and dd: wind direction

Table 4 Stability classes for the data analysis

1.	Unstable			L^{-1}	$<$	$-(200\,\mathrm{m})^{-1}$
2.	Slightly unstable	$-(200\,\mathrm{m})^{-1}$	$\leq$	L^{-1}	$<$	0
3.	Slightly stable	0	$<$	L^{-1}	$\leq$	$(200\,\mathrm{m})^{-1}$
4.	Stable	$(200\,\mathrm{m})^{-1}$	$<$	L^{-1}		

Table 5 Numbers of 30-min runs for the analysis of the momentum flux

Stability class	Height (m)	Wind direction sector				All sectors
		1	2	3	4	
Unstable	20	260	39	121	210	630
	100	315	33	124	214	686
	180	247	60	110	98	515
	All heights	822	132	355	522	1831
Slightly unstable	20	227	82	45	177	531
	100	243	12	44	161	460
	180	198	85	42	104	429
	All heights	668	179	131	442	1420
Slightly stable	20	113	93	26	213	445
	100	141	5	27	177	350
	180	109	98	27	130	364
	All heights	363	196	80	520	1159
Stable	20	231	167	318	357	1073
	100	295	118	299	371	1083
	180	250	211	308	262	1031
	All heights	776	496	925	990	3187
	Totals	2629	1003	1491	2474	7597

the wind speed gradient must be positive. The large number of rejected cases reveals that a significant portion of the measurements, especially at the 100- and 180-m levels in stable conditions, were made well above the surface layer.

The surface-layer Obukhov length (L_{SL}) has been used to separate the dataset into four stability classes (see Table 4). The distribution of the runs over the stability and wind direction classes is given in Tables 5 and 6, showing that stable conditions prevailed during the measuring campaign. The number of runs in the east sector is substantially less than for the other sectors.

To determine at what time of day the selected stability subsets are taken, $\cos(2\pi\ t/2400)$ and $\sin(2\pi\ t/2400)$, where t is time, are averaged for each subset. The phase angle of the resulting vector indicates the preferential time and its length is a

Table 6 Numbers of 30-min runs for the analysis of the sensible heat flux

Stability class	Height (m)	Wind direction sector				All sectors
		1	2	3	4	
Unstable	20	225	33	78	113	479
	100	315	28	106	200	649
	180	217	36	89	91	433
	All heights	787	97	273	404	1561
Slightly unstable	20	220	82	38	101	441
	100	243	10	44	155	452
	180	153	76	36	102	367
	All heights	616	168	118	358	1260
Slightly stable	20	111	93	21	149	374
	100	141	4	26	173	344
	180	88	96	22	130	336
	All heights	340	193	69	452	1054
Stable	20	219	164	210	228	821
	100	295	100	286	351	1032
	180	190	147	262	244	843
	All heights	704	411	758	823	2696
	Totals	2447	869	1218	2037	6571

measure of this preference. Where all events occur at the same time the vector would have unit length, and where the events are randomly distributed over time the vector would have a length close to zero. For all k-vane heights and wind direction sectors together the results are (1146, 0.77) for unstable, (1236, 0.58) for slightly unstable, (2140, 0.14) for slightly stable and (2307, 0.57) for stable conditions. It is clear that the (slightly) unstable subset comprises many samples taken round or before noon, when the ABL is probably shallow and rapidly growing. In those cases the selection of wind speeds larger than $3\,\mathrm{m\,s^{-1}}$ favours conditions with strong entrainment (Driedonks and Tennekes 1984, Pino et al. 2003). The stable subset is dominated by samples taken round midnight and the slightly stable subset has a small surplus of samples taken in the early evening.

Malfunction of the k-vanes has been a serious problem, whose main cause has been frequent breakdown of the electronics in the photochopper of the propeller. Other causes of data drop-out were short-circuit in the thermocouple amplifiers, broken thermocouples by rain or hail and computer failure.

5 Wind profiles and Fluxes

Profiles of wind speed (U), normalized with the wind speed at 200 m, are plotted in Fig. 2 for all wind direction sectors and stability classes. Regarding the wind direction sector and stability class, each measuring point comprises at least 5 runs (usually much more). The ratio (R) of the wind speed at height z to that at 200 m has been calculated by fitting the equation $U_z = RU_{200}$ using a χ^2-procedure. The uncertainty in U is assumed to be 10% in this analysis, with the uncertainty of the 10% percentile wind speed in the dataset as a minimum.

From the velocity profiles it can be seen that the retardation of the wind speed is the strongest in the southern sector, although the eastern sector is usually considered

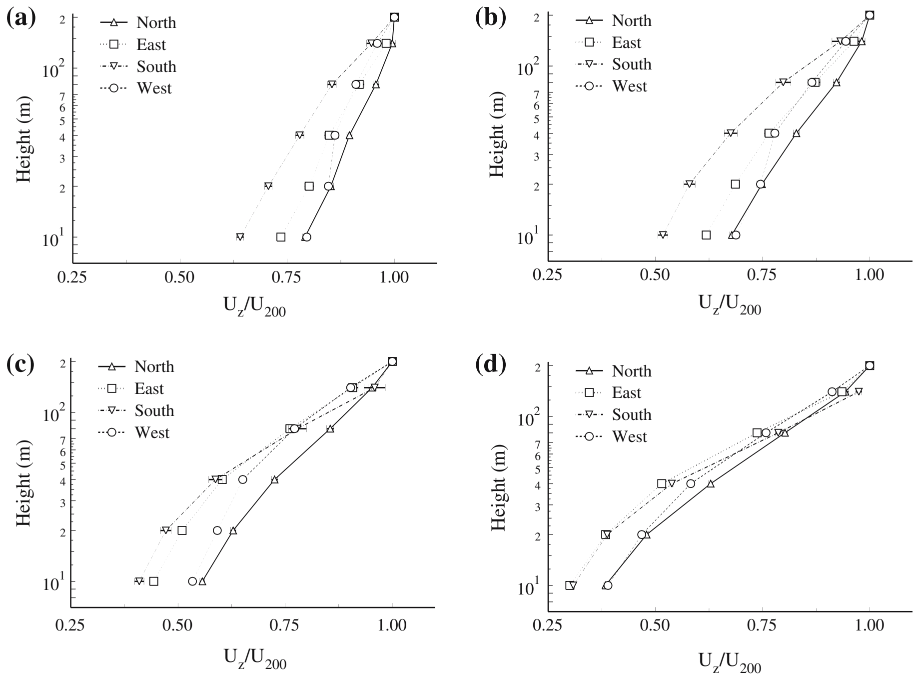

Fig. 2 Scaled wind speed U_Z/U_{200} as a function of height derived from the routine Cabauw measurement separated into four wind direction sectors: (**a**) Unstable; (**b**) Slightly unstable; (**c**) Slightly stable; (**d**) Stable

to be the roughest sector. In the northern sector the retardation is comparable to that of the western sector, which is considered to be the smoothest. Also evident is the strong curvature in these profiles, especially in stable conditions. At 40 m, in (slightly) unstable and slightly stable conditions, a kink in the velocity profile can be seen in the western sector suggesting a rough-to-smooth transition in surface roughness.

Ratios of friction velocity measured by k-vanes to that of the surface-layer value are plotted in Fig. 3. In the unstable, well-mixed ABL $u_{*\mathrm{kv}}$ is close to $u_{*\mathrm{SL}}$ and can be considered approximately constant with height. The relative momentum flux divergence increases with increasing stability, and in the stable ABL u_* at 180 m has decreased to 50% of its surface value. The divergence shows that the measurements at 100 m and 180 m height are made well above the surface layer. In the eastern direction $u_{*\mathrm{kv}}$ at 20 m is larger than $u_{*\mathrm{SL}}$ for all stabilities. In this direction the upstream fetch is heavily disturbed close to the tower. This is reflected in the $u_{*\mathrm{kv}}$ measurements, while $u_{*\mathrm{SL}}$ represents a large-scale friction velocity. In the west and in the south direction, where there are few obstacles in the tower's vicinity, $u_{*\mathrm{kv}}$ is smaller than $u_{*\mathrm{SL}}$ at 20 m.

In general Monin–Obukhov similarity theory is based on the assumption that momentum and heat fluxes do not change throughout the surface layer, and the surface layer is defined as the 'constant flux layer'. Figure 3 shows that there is a strong momentum flux divergence, except for the unstable cases. A strong divergence was also found for the sensible heat flux (Fig. 4). The daytime flux divergence (unstable conditions) may partially be caused by entrainment. The data selection excludes low wind speeds and consequently low friction velocities to ensure that the k-vanes are

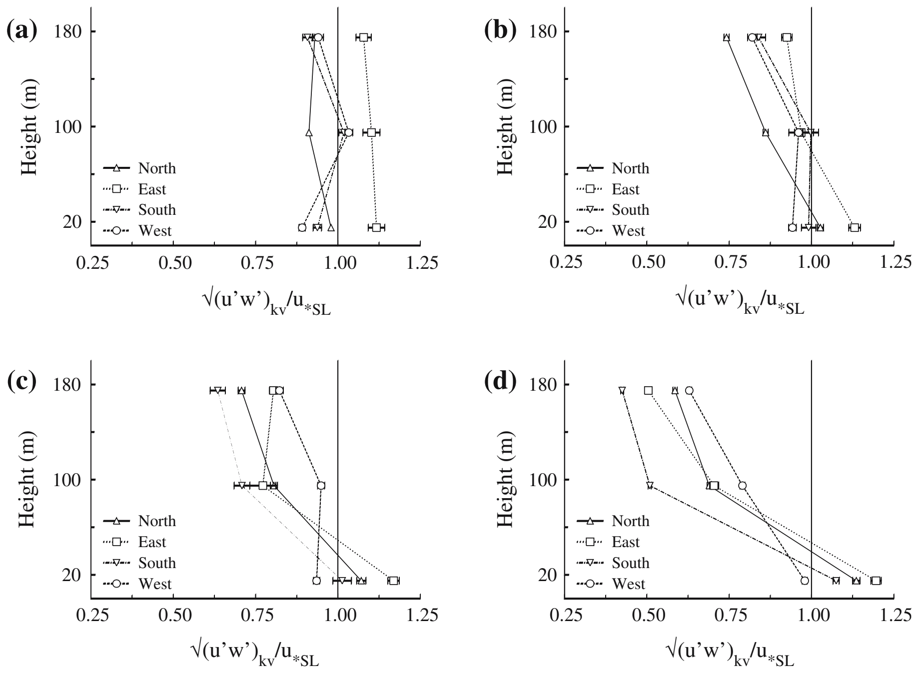

Fig. 3 Friction velocity as measured by the k-vanes normalized with the surface-layer friction velocity as a function of height and separated into four wind direction sectors: (**a**) Unstable; (**b**) Slightly unstable; (**c**) Slightly stable; (**d**) Stable

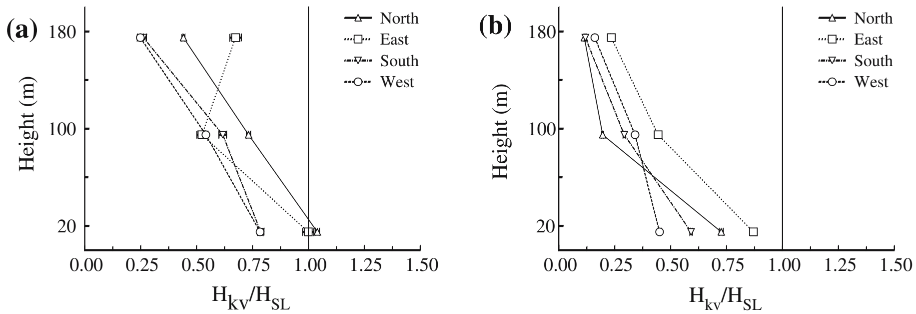

Fig. 4 Sensible heat flux as measured by the k-vanes normalized with the surface-layer sensible heat flux as a function of height and separated into four wind direction sectors: (**a**) Unstable; (**b**) Stable

operating properly. Moreover, the dataset includes many situations with an unstable, shallow boundary layer in the early morning hours with a growing convective boundary layer. These conditions are in favour of entrainment and the entrainment heat flux can be about 20%–50% of the surface heat flux (Driedonks and Tennekes 1984, Pino et al. 2003). With an ABL height of 500 m the heat flux may become zero at a height of only 400 m. The divergence in momentum and heat fluxes shows that our measurements are often done above the surface layer, so we cannot expect that Monin–Obukhov similarity theory is still applicable here.

Let us explore therefore the dimensionless wind speed gradient using $\partial U/\partial z$ from the tower measurements:

$$\phi_m\left(\frac{z}{L}\right) = \frac{kz}{u_*}\frac{\partial U}{\partial z}. \tag{1}$$

Here we analyse our data by using both the local values for u_* and L (so called local scaling) as well as the surface-layer values for u_* and L. Since the fluxes become smaller with height and the scatter increases as well, only the k-vane fluxes at 20 m and 100 m are analysed. Following Nieuwstadt (1984), the wind speed profile is fitted to the function $U = a_1 + a_2 z + a_3 z^2 + a_4 \ln z$, and from this fitted profile $\partial U/\partial z$ is computed at 20 m or 100 m. The averages of z/L and ϕ_m are plotted in Figs. 5a and 5c for the surface-layer scaling results, where the data have been averaged in bins each containing 20 runs. The standard deviation of the mean of ϕ_m has been plotted as an error bar. For comparison Dyer's (1974) stability function is also plotted. In addition to the usual data selection, positive wind speed gradients were required ($\partial U/\partial z > 0$), and cases with $u_* < 0.15\,\mathrm{m\,s^{-1}}$ were rejected to ensure that ϕ_m is well defined.

At 20 m ϕ_m is lower than Dyer (1974), and only in the south direction, the most complex and roughest sector, in unstable conditions is ϕ_m larger than Dyer (1974). With increasing stability the difference between ϕ_m and Dyer (1974) increases. At 100 m there are less measuring points, especially in the eastern sector where there are few. The scatter in the data is also larger. In all directions ϕ_m has increased compared to the 20-m level. In the north and west directions ϕ_m is still close to Dyer (1974) for neutral and unstable cases, and in the southern sector ϕ_m is far above Dyer (1974) over the whole range of stabilities.

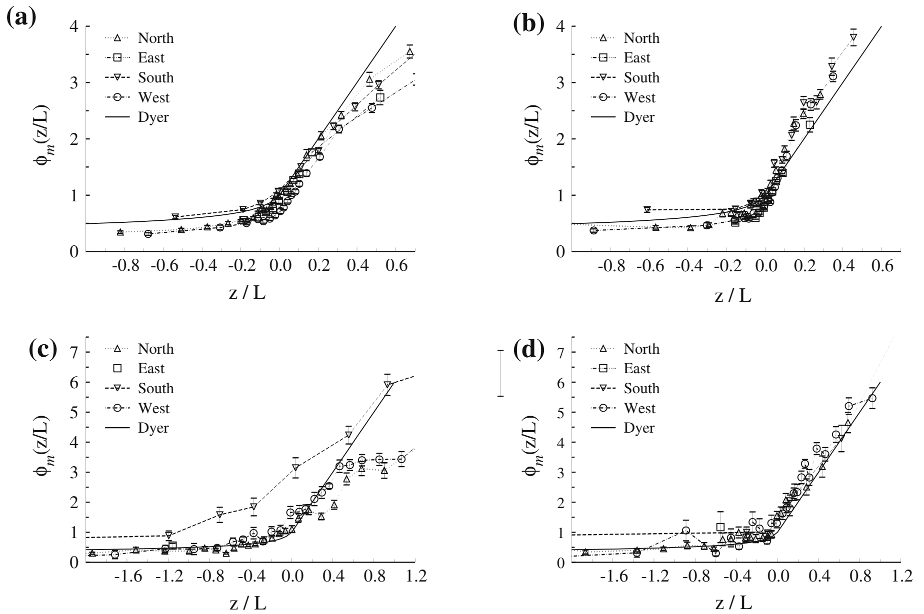

Fig. 5 Dimensionless wind speed gradient as a function of stability calculated from k-vane fluxes at 20 m and 100 m, and separated into four wind direction sectors: (**a**) Surface-layer scaling, 20 m; (**b**) Local scaling, 20 m; (**c**) Surface-layer scaling, 100 m; (**d**) Local scaling, 100 m

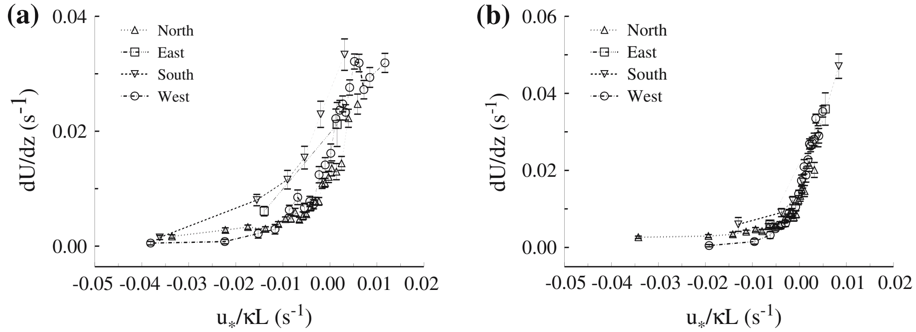

Fig. 6 As Fig. 5 but here for the wind speed gradient dU/dz versus $u_*/\kappa L$ at 100 m: (**a**) Surface-layer scaling; (**b**) Local scaling

In Eq. (1) u_* and L can also be computed from the k-vane measurements (local scaling). As shown in Figs. 5b and 5d local scaling reduces the scatter in ϕ_m considerably. At both 20 m and 100 m ϕ_m collapses to a single curve, also for the southern sector. In neutral and unstable cases ϕ_m is still below Dyer (1974) at 20 m. Although the fluxes at 20 m are still close to their surface-layer values, Fig. 5b shows that local scaling performs slightly better, especially in stable cases. Figure 5d shows that at 100 m local scaling performs much better than surface-layer scaling. Figures 3a and 4a show that at 100 m the difference between surface-layer scaling and local scaling is primarily caused by the difference in heat flux.

Note that ϕ_m and z/L both contain the factor $\kappa z/u_*$ (see Eq. (1)). Consequently the correlation that is found in Fig. 5 may partially be an artefact. In Fig. 6 dU/dz is plotted against $(u_*/\kappa z)(z/L) = \kappa u_*/L = (g/\theta)\overline{w'\theta'}/u_*^2$ for the 100-m level for surface-layer and local scaling, which should be free of artificial correlation. Figure 6 confirms that the good performance is not artificial and that there is less scatter when local scaling is used.

6 Roughness lengths

In this section several methods to determine the aerodynamic roughness length (z_0) are compared. The roughness length can be computed from wind speed profiles, gustiness analysis, and the drag coefficient. All these methods may result in different estimates of z_0 as they have different source areas.

The footprint or source area is the surface effectively determining the level or gradient of a meteorological parameter downstream. It can be described by sophisticated weighting functions and is a function of height, stability, and roughness itself. In neutral conditions the area with the maximum contribution lies upwind at a distance of about ten times the measuring height. The source area is about 20°–30° wide. Increasing atmospheric instability reduces the source area to an area closer to the evaluation point (Van Ulden 1978, Schmid and Oke 1990, Horst 1999, Schmid and Lloyd 1999, Kljun et al. 2004).

The larger the source area of a meteorological parameter, the more this entity will represent a large-scale average. The largest eddies in the ABL are also those that adapt slowest of all to changes in surface properties (Højstrup 1981, Beljaars 1987b). The longitudinal velocity variance in the surface layer (σ_u^2) is mostly determined by the largest eddies, and for that reason $z_{0\mathrm{std}}$ is expected to represent the best large-scale average of the roughness length.

6.1 Roughness lengths from profiles

Using Nieuwstadt's (1978) method the wind speed profile at Cabauw is analysed as a function of wind direction. Nieuwstadt minimized the function

$$\Phi\left(u_*,\theta_*\right) = \Phi_u/\Delta u^2 + \Phi_\theta/\Delta\theta^2, \tag{2}$$

where

$$\Phi_u = \sum_{i=2}^{N_U}\left[U_{z_i} - U_{z_{\mathrm{ref}}} - u\left(z_i,u_*,\theta_*\right) + u(z_{\mathrm{ref}},u_*,\theta_*)\right]^2, \tag{3}$$

and

$$\Phi_\theta = \sum_{j=2}^{N_\theta}\left[\theta_{z_j} - \theta_{z_{\mathrm{ref}}} - \theta(z_j,u_*,\theta_*) + \theta(z_{\mathrm{ref}},u_*,\theta_*)\right]^2. \tag{4}$$

Here Δu and $\Delta\theta$ are the measuring errors in the wind speed U and temperature θ respectively, and $\theta_* = -H/\rho c_p u_{*\mathrm{prof}}$ is the temperature scale, where $u_{*\mathrm{prof}}$ is the profile derived friction velocity, $u(z,u_*,\theta_*)$ and $\theta(z,u_*,\theta_*)$ are the log-linear functions for wind speed and temperature and N_U and N_θ are the number of heights at which wind speed and temperature are measured, respectively. The subscript 'ref' refers to the lowest level used in the profiles. Nieuwstadt used estimated values of z_0 and added $U\left(z_0\right) = 0$ to his profile. We will not do so, as the profiles are used to determine z_0. Dyer's (1974) stability functions and the integrated log-linear functions Ψ_M and Ψ_H as presented by Garratt (1992) are adopted here. For U the total horizontal wind vector has been used. The fitted wind speed profile is extrapolated to $U(z_0) = 0$ to derive the roughness length. Any zero plane displacement, which is expected to be small and of minor importance when computing z_0, is neglected (Nieuwstadt 1978, Kustas and Brutsaert 1986, Grant and Mason 1990, Grant 1991). In addition to the basic selection criteria, we applied the criteria of Korrell et al. (1982) as well and we analysed only the slightly unstable cases.

In Fig. 7a the resulting roughness length $z_{0\mathrm{prof}}$ is plotted. It is computed using two different height intervals: 10–40 m and 40–200 m. Every point represents the average over 30 estimates of $z_{0\mathrm{prof}}$. For comparison $z_{0\mathrm{std}}$ is plotted as well. Figure 7a shows that the higher profile yields similar roughness lengths to $z_{0\mathrm{std}}$ in most directions where, apparently, the 40-m level is not influenced by the rough-to-smooth transition close to the tower. Only in the south-western sector $z_{0\mathrm{prof}}$ decreases to values that are far too low to be realistic. In this direction the roughness length is smaller than 1 mm. Such small roughness lengths can only be found over very smooth surfaces (water, sand, snow-covered land), and indicates that the profiles in this sector at Cabauw are strongly disturbed. The lower profile yields smaller roughness lengths than the higher profile except for the sectors from west to north. This profile also yields very low z_0 values in the south-west direction. In most directions the undisturbed fetch is not long enough, less than a few hundreds of metres, for the local internal boundary layer

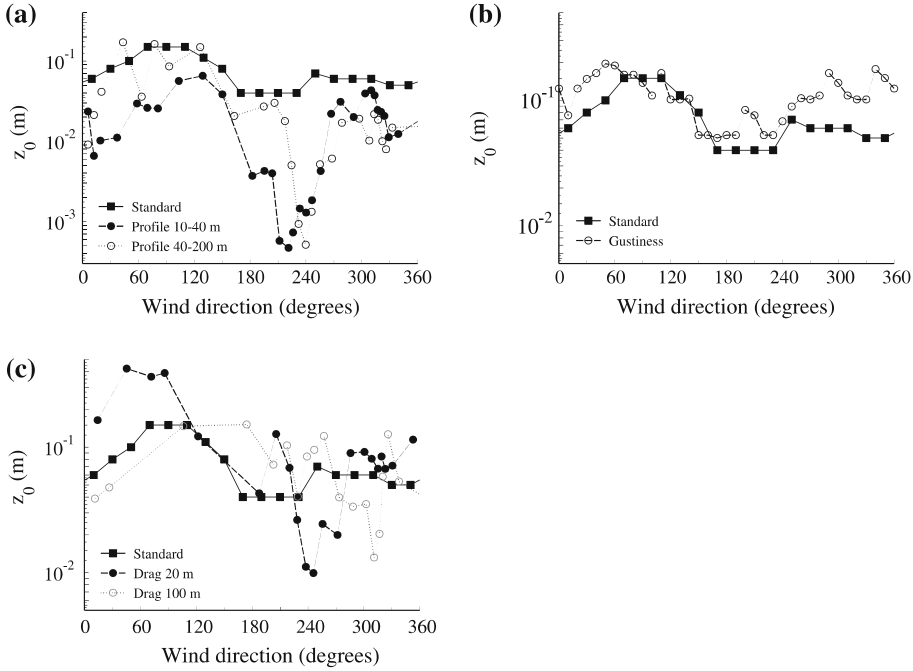

Fig. 7 Roughness length as a function of wind direction estimated using various methods at the Cabauw site, $z_{0\mathrm{std}}$ is plotted as a standard reference: (**a**) Profile measurements using different height intervals; (**b**) Gustiness measurements at 10 m; (**c**) Drag coefficient measurements at 20 m and 100 m

(IBL) to reach the 10-m level. However, in the south-west direction the undisturbed fetch is longer (0.5–2 km), resulting in a very low estimate of $z_{0\mathrm{prof}}$. The low $z_{0\mathrm{prof}}$ in the upper profile shows that the local IBL has reached the 40-m level in the direction 240°. The unrealistically low z_0 values in the lower profile, however, show that the equilibrium boundary layer has not yet reached the 40-m level in this direction. Figure 7a also shows that directions with distinct roughness values can be very narrow, indicating that the source areas for these measurements are very narrow as well.

6.2 Roughness lengths from the drag coefficient

The drag coefficient, $C_\mathrm{d} \equiv (u_*/U)^2$, can be used to estimate the roughness length using the logarithmic wind speed profile. From the logarithmic wind speed profile it follows that C_d is a function of z, z_0, and stability:

$$\sqrt{C}_\mathrm{d} = \frac{\kappa}{\ln z/z_{0\mathrm{drag}} - \Psi_M\,(z/L) + \Psi_M\left(z_{0\mathrm{drag}}/L\right)}. \tag{5}$$

An advantage of this approach is that measurements need to be done only at a single level. A disadvantage is the need for measurements or estimates of the momentum flux. Fortunately, u_* can be estimated from σ_u or the gustiness, and both can be assessed by regular anemometers. The routine Cabauw roughness length as shown in Fig. 7a is an example of the application of this method (Wieringa 1976, Verkaik 2000).

From the present dataset the roughness lengths found from direct observations of u_*/U or the gustiness can be compared to those from σ_u. The gustiness derived roughness length ($z_{0\text{gust}}$) has been calculated for 10°-wide bins using the routine measurements at 10-m height. In Fig. 7b $z_{0\text{gust}}$ is plotted and compared to $z_{0\text{std}}$. For most directions $z_{0\text{gust}}$ is similar or larger than $z_{0\text{std}}$, and compared to $z_{0\text{prof}}$ it shows very little directional variation.

From the k-vane measurements of the drag coefficient at 20-m and 100-m heights $z_{0\text{drag}}$ has been calculated using the same data selection as for the profiles. Figure 7c shows that the directional variation in $z_{0\text{drag}}$ is larger than that of $z_{0\text{std}}$ and $z_{0\text{gust}}$. The peak in the north-east direction is caused by farms and trees at 300 m distance and likewise it is possible to indicate more surface features producing the variation of $z_{0\text{drag, 20m}}$: the peak at 190° is caused by trees and orchards (0.5–1.5 km), and further still to the south there is a sector overlooking the river bed, which is a smooth area. The south-west direction has the largest undisturbed fetch over grassland and the roughness length found here is in the order of several tens of mm which corresponds well to z_0 values reported in the literature (Wieringa 1993).

At 100 m $z_{0\text{drag}}$ is in the range 0.01–0.10 m for most directions. The 100-m roughness length shows a noisy profile in the west direction. However, assuming that the 100-m observations are not influenced by the closest windbreaks, the low z_0 in direction 300° coincides with a very smooth upwind fetch starting $\simeq$1 km from the tower (see Fig. 1). The low z_0 in the north direction, however, cannot be explained easily. In the east direction z_0 is clearly smaller at 100 m than at 20 m, indicating that the 100-m footprint is mainly overlooking the village Lopik in the east.

7 Discussion

7.1 Flux–profile relationships

Roughness transitions can cause ϕ_m to deviate from its regular value. A low ϕ_m indicates that $\partial U/\partial z$ is small compared to u_*, typical for a rough-to-smooth roughness change (Rao et al. 1974). ϕ_m is lower than Dyer (1974) in most directions at 20 m when using surface-layer scaling and also using local scaling in unstable cases. Fig. 5a can be compared with Figs. 5 and 7 from Beljaars et al. (1983) where also low values for ϕ_m were found.

Deviations of the regular flux–profile relationships in very stable conditions using surface-layer scaling have been observed frequently. Local scaling has been more successful in these cases (Holtslag and Nieuwstadt 1986, Holtslag and De Bruin 1988, Beljaars and Holtslag 1991, Vickers and Mahrt 1999). Local scaling can also be applied to ϕ_m in unstable conditions at homogeneous sites (Sorbjan 1986, Yumao et al. 1997). Figures 5b and 5d, however, show that local scaling of ϕ_m also applies above the surface layer, in the disturbed ABL at Cabauw. If the underestimation of ϕ_m at 20 m is explained by the rough-to-smooth transition, then Fig. 5d shows that at 100 m the flux–profile relationships seem to reflect an equilibrium ABL as long as local scaling is applied.

Comparing eddy-correlations measurements at 3.5 m and 22.5 m Beljaars et al. (1983) found that there is an increase in friction velocity with height, except for those directions that are really free of obstacles. Heat and moisture fluxes are about the same at both levels for all directions. These observations confirmed the assumptions of Beljaars (1982), firstly, that the heat flux throughout the surface layer is constant in spite of perturbed profiles, and secondly, that the exchange coefficients for momentum and heat are modified in the same way by obstructions. The success of local scaling suggests that these arguments still hold at 100 m despite the strong flux divergence.

Our data selection for unstable conditions is in favour of situations with a developing boundary layer in the morning hours in combination with wind shear. The strong heat flux divergence in unstable conditions indicates that the boundary layer is heating up (Fig. 4). Moreover, the entrainment rate is expected to be relatively high (Pino et al. 2003), so the heat flux becomes negative at a relatively low height. At the same time the momentum flux is enhanced by entrainment in the upper part of the ABL. This explains why, in contrast to the heat flux, there is little divergence in momentum flux (Fig. 3).

7.2 Wind speed profiles and local roughness

The rough-to-smooth transition at Cabauw is evident from a kink in the neutral wind speed profile. The kink is best seen in the west sector (Fig. 2), where the extent of the obstacle-free fetch is large enough for the IBL to reach the 20-m level. For most directions the present dataset is too coarse to do a detailed analysis of the IBL structure of the Cabauw site. From earlier research is was found that near-neutral wind speed profiles at Cabauw show a kink around 20 m in the south-west direction, and around 10 m in the east direction. Both the lower and upper parts of the profile are logarithmic (Beljaars 1982). Wieringa (1976) reported that the upper profiles corresponded to the gustiness derived roughness lengths, as confirmed by Fig. 7b.

At Cabauw the friction velocity is routinely computed from the large-scale roughness $z_{0\mathrm{drag}}$ and the wind speed at 10 m. For most directions this method is accurate. However, in the south-west sector the 10-m wind is well within the local IBL. Here the wind speed is adapted to the smooth grass-covered land, whereas the roughness length still represents the high, large-scale average. This results in an apparent overestimation of the friction velocity and hence the wind speed (gradient), as seen in Nieuwstadt (1978).

Nieuwstadt (1978) compared the friction velocity from his profile method with direct flux measurements at 20 m, and found good agreement for most directions. However, for the south-west direction the directly measured u_* was smaller than that from the profiles. Nieuwstadt added the large-scale roughness length as an additional measuring point to the profile ($U(z_{0\mathrm{std}}) = 0$), and he used $z_0 = 0.07$ m for the south-west direction. Nieuwstadt suggested that this roughness length was too high, causing the overestimation of the profile-derived u_*. Actually, the roughness length used by him was not too high, but corresponded only to the upper profile and so did the estimated u_*: the 20-m level is within the local IBL in the south-west direction and the measured u_* is lower than the friction velocity of the upper profile.

Meteorological research masts are often placed at sites selected for their undisturbed terrain. Therefore the local roughness is usually smaller than the large-scale roughness. Cabauw is such an example, but at the Boulder tower in Colorado similar results are found (Korrell et al. 1982, Bowen 2000).

7.3 Roughness footprints

Significant differences in roughness length are found from different height intervals for the wind speed profiles, or when the roughness length is computed from the gustiness, turbulence intensity, or the drag coefficient. The differences have to be explained by the differences in footprint between these methods in combination with the inhomogeneities of the Cabauw environment.

The source area for the 10–40 m profile is expected to be similar to those for eddy-covariance measurements done at $\sqrt{z_{\text{high}} z_{\text{low}}} = 20\,\text{m}$, where the source area weight function falls off rapidly at a distance of 0.5–1 km (Horst 1999). On this scale the Cabauw environment is very disturbed resulting in a very changeable lower profile $z_{0\text{prof}}$ (Fig. 7a). The $z_{0\text{drag}}$ is much less changeable with direction (Fig. 7c). Only in the south-west direction, where the IBL over smooth grass encloses the 20-m level, does $z_{0\text{drag}}$ represent the local roughness of grass. A similar difference in momentum flux between 3.5 m and 22.5 m height was found by Beljaars et al. (1983). Later Schmid and Oke (1990) showed that the source area for the 22.5-m level comprises many obstacles upstream, while for the 3.5-m level the source area is much smoother. So, although the footprints of $z_{0\text{drag}}$ and the lower $z_{0\text{prof}}$ are expected to be similar, the presence of the local IBL causes large differences in roughness length. The IBL reaches the 10-m measuring point in most directions, while it reaches the 20-m measuring point only in the south-west direction.

From the spectral point of view gusts are the result of the superposition of several eddies of different sizes. Whereas the largest eddies contribute most significantly to σ_u, the gust is also determined by smaller eddies because of the small time scale of gusts. This means that the source area for $z_{0\text{gust}}$ may also be a superposition of large-scale and local roughness. Figure 7c shows that $z_{0\text{gust}}$ is exceeded by $z_{0\text{drag}}$ in directions where nearby obstacles are present. In other directions it is comparable to $z_{0\text{std}}$. There seems to be a correlation, however, between $z_{0\text{gust}}$ and $z_{0\text{drag}}$: every peak in $z_{0\text{drag}}$ is accompanied by a peak in $z_{0\text{gust}}$. So, the footprint of $z_{0\text{gust}}$ seems to be superposition of local and large-scale roughness indeed, and its footprint is larger than that of $z_{0\text{drag}}$.

8 Summary and conclusions

Our results show that the k-vanes are capable of measuring momentum fluxes with sufficient accuracy provided that they are not used at low altitudes. However, the k-vanes proved vulnerable to atmospheric electricity and contamination of the bearings supporting the propellers.

The analysis presented in this study of the wind speed profiles and the roughness length generally confirms the conclusions of earlier studies at Cabauw. The wind speed profiles at Cabauw are disturbed by the rough-to-smooth transition that is found at a distance that depends on the wind direction. Only in the south-west direction does the obstacle-free fetch extend so far that the equilibrium boundary layer over the grass covered land reaches high enough to enclose the flux measurements at 20 m.

In addition, we have analysed the momentum and heat fluxes up to heights of 100 m along the tower not explored before. Except for unstable cases the momentum flux in our data selection shows significant divergence, and the heat flux divergence is even more pronounced. Our dataset comprises many cases where the measurements are made above the surface layer. Moreover, in unstable conditions the entrainment rate is expected to be high, due to our data selection procedure that is in favour of conditions with a developing boundary layer in the morning hours with significant shear. It is reconfirmed that in the stable boundary layer the regular flux–profile relationships are valid provided that local scaling is used. Also in unstable conditions it appears that scaling of the profiles with local fluxes works well, even for the disturbed ABL above the surface layer.

We analysed the roughness lengths using three methods. This showed that every method has his own footprint resulting in different estimates of the roughness length depending on the method used. The roughness lengths derived at Cabauw from wind speed profiles depend strongly on the height range over which the profile is taken. The lower profiles (<40 m) are disturbed by the IBL caused by the local rough-to-smooth transition. Roughness lengths from these profiles are completely invalid. The higher profile yields roughness lengths that can be considered area-averaged values, provided that the lower measuring points are not disturbed by the local IBL. Gustiness derived roughness lengths seem to aggregate both nearby and distant roughness elements and are often the largest of the roughness estimates examined here. The roughness from drag coefficients exhibits more local characteristics than the gustiness. However, if the drag coefficient is measured above the local IBL it yields roughness values that are close to the large-scale area-average. At inhomogeneous sites such as Cabauw the roughness length can be estimated best by measuring the drag coefficient just above the local IBL. Indirect ways for determining the drag coefficient such as measurements of the gustiness or the standard deviation of horizontal wind speed fluctuations give similar results. These methods are less sensitive to local disturbances of the surface layer than profile derived roughness lengths, which are easily disturbed by terrain inhomogeneities resulting in unrealistic values.

Acknowledgements This project was undertaken by the Meteorology and Air Quality Section of Wageningen University (WU) in collaboration with the Royal Netherlands Meteorological Institute (KNMI). It was originally initiated under the supervision of Prof. Dr. J. Wieringa. We are indebted to the technical staff of both KNMI (Sjaak Koster and Frans Renes among others), and WU (Bert Heusinkveld and Frits Antonysen among others), for helping setting up the k-vane measurements. Also thanks to the scientific staff of the Atmospheric Research group of KNMI for making available the profile data. Special thanks to Fred Bosveld for providing the data acquisition software. The investigations were (in part) supported by the Netherlands Organization for Scientific Research (NWO), project no. 750.194.15.

References

Beljaars ACM (1982) The derivation of fluxes from profiles in perturbed areas. Boundary-Layer Meteorol 24:35–55

Beljaars ACM (1987a) The influence of sampling and filtering on measured wind gusts. J Atmos Oceanic Technol 4:613–626

Beljaars ACM (1987b) On the memory of wind standard deviation for upstream roughness. Boundary-Layer Meteorol 38:95–101

Beljaars ACM (1988) The measurement of gustiness at routine wind stations – a review. In: WMO-TECO-1988. Leipzig, pp 311–316. WMO/TD-No. 222, also Royal Netherlands Meteorological Institute, Sc. Rep., WR 87-11

Beljaars ACM, Bosveld FC (1997) Cabauw data for the validation of land surface parameterization schemes. J Climate 10:1172–1193

Beljaars ACM, Holtslag AAM (1991) Flux parameterization over land surfaces for atmospheric models. J Appl Meteorol 30:327–341

Beljaars ACM, Schotanus P, Nieuwstadt FTM (1983) Surface layer similarity under nonuniform fetch conditions. J Clim Appl Meteorol 22:1800–1810
Bowen BM (2000) Near-neutral surface layer turbulence at the Boulder atmospheric observatory tower: evidence of increasing vertical turbulence with height. J Appl Meteorol 39:716–724
De Wit AJW, Van der Heijden TGC, Thunnissen HAM (1999) Vervaardiging en nauwkeurigheid van het LGN3 grondgebruiksbestand. DLO-Staring Centrum, Wageningen, 84 pp (in Dutch)
Driedonks AGM, Tennekes H (1984) Entrainment effects in the well-mixed atmospheric boundary layer. Boundary-Layer Meteorol 30:75–105
Dyer AJ (1974) A review of flux-profile relationships. Boundary-Layer Meteorol 7:363–372
Garratt JR (1992) The atmospheric boundary layer. Cambridge University Press, Cambridge, 316 pp
Grant ALM (1991) Surface drag and turbulence over an inhomogeneous land surface. Boundary-Layer Meteorol 56:309–337
Grant ALM, Mason PJ (1990) Observations of the boundary-layer structure over complex terrain. Quart J Roy Meteorol Soc 116:159–186
Højstrup J (1981) A simple model for the adjustment of velocity spectra in unstable conditions downstream of an abrupt change in roughness and heat flux. Boundary-Layer Meteorol 21:341–356
Holtslag AAM (1984) Estimation of diabatic wind speed profiles from near-surface weather observations. Boundary-Layer Meteorol 29:225–250
Holtslag AAM, De Bruin HAR (1988) Applied modelling of the nighttime surface energy balance over land. J Appl Meteorol 27:689–704
Holtslag AAM, Nieuwstadt FTM (1986) Scaling the atmospheric boundary layer. Boundary-Layer Meteorol 36:201–209
Horst TW (1999) The footprint for estimation of atmosphere-surface exchange fluxes by profile techniques. Boundary-Layer Meteorol 90:171–188
Kljun N, Calanca P, Rotach MW, Schmid HP (2004) A simple parameterisation for flux footprint predictions. Boundary-Layer Meteorol 112:503–523
Korrell A, Panofsky HA, Rossi RJ (1982) Wind profiles at the Boulder tower. Boundary-Layer Meteorol 22:295–312
Kustas WP, Brutsaert W (1986) Wind profile constants in a neutral atmospheric boundary layer over complex terrain. Boundary-Layer Meteorol 34:35–54
Monna WAA, Van der Vliet JG (1987) Facilities for research and weather observations on the 213 m tower at Cabauw and remote locations. Scientific Report WR 87-5, Royal Netherlands Meteorological Institute, 27 pp
Nieuwstadt FTM (1978) The computation of the friction velocity u_* and the temperature T_* from temperature and wind velocity profiles by least-square methods. Boundary-Layer Meteorol 14:235–246
Nieuwstadt FTM (1984) The turbulent structure of the stable, nocturnal boundary layer. J Atmos Sci 41:2202–2216
Pino D, Vilá-Guerau de Arellano J, Duynkerke PG (2003) The contribution of shear to the evolution of a convective boundary layer. J Atmos Sci 60:1913–1926
Rao KS, Wyngaard JC, Coté OR (1974) The structure of the two-dimensional internal boundary layer over a sudden change of surface roughness. J Atmos Sci 31:738–746
Schmid HP, Lloyd CR (1999) Spatial representativeness and the location bias of flux footprints over inhomogeneous areas. Agric Forest Meteorol 93:195–209
Schmid HP, Oke TR (1990) A model to estimate the source area contribution to turbulent exchange in the surface layer over patchy terrain. Quart J Roy Meteorol Soc 116:965–988
Sorbjan Z (1986) On similarity in the atmospheric boundary layer. Boundary-Layer Meteorol 34:377–397
Steeneveld G-J, Holtslag AAM, De Bruin HAR (2005) Fluxes and gradients in the convective surface layer and the possible role of boundary-layer depth and entrainment flux. Boundary-Layer Meteorol 116:237–252
Van der Vliet JG (1998) Elf jaar Cabauw-metingen. Technical Report TR-210, Royal Netherlands Meteorological Institute, 79 pp (In Dutch)
Van Ulden AP (1978) Simple estimates for vertical diffusion from sources near the ground. Atmos Environ 12:2125–2129

Van Ulden AP, Wieringa J (1996) Atmospheric boundary layer research at Cabauw. Boundary-Layer Meteorol 78:39–69
Verkaik JW (1998) Evaluation of the K-Gill propeller vane. J Atmos Oceanic Technol 15:901–915
Verkaik JW (2000) Evaluation of two gustiness models for exposure correction calculations. J Appl Meteorol 39:1613–1626
Vickers D, Mahrt L (1999) Monin-Obukhov similarity theory in the coastal zone. In: Preprints, 13th symp. on boundary layers and turbulence. Amer Meteorol Soc Dallas, TX, pp 407–410
Wessels HRA (1983) Distortion of the wind field by the Cabauw meteorological tower. Scientific Report WR 83-15, Royal Netherlands Meteorological Institute, 34 pp
Wessels HRA (1984) Cabauw meteorological data tapes 1973–1984; description of instrumentation and data processing for the continuous measurements. Scientific Report WR 84-6, Royal Netherlands Meteorological Institute, 23 pp
Wieringa J (1976) An objective exposure correction method for average wind speeds measured at a sheltered location. Quart J Roy Meteorol Soc 102:241–253
Wieringa J (1993) Representative roughness parameters for homogeneous terrain. Boundary-Layer Meteorol 63:323–363
Yumao X, Chaofu Z, Zhongkai L, Wei Z (1997) Turbulent structure and local similarity in the tower layer over the Nanjing area. Boundary-Layer Meteorol 82:1–21